Chemical Physics Letters 641 (2015) 173–180

Contents lists available at ScienceDirect

Chemical Physics Letters

journal homepage: www.elsevier.com/locate/cplett

Benchmark calculation for tunnelling through a multidimensional asymmetric double well potential

James A. Green*, Dmitrii V. Shalashilin

School of Chemistry, University of Leeds, Leeds LS2 9JT, United Kingdom

ARTICLE INFO

Article history:
Received 16 September 2015
In final form 28 October 2015
Available online 10 November 2015

ABSTRACT

A benchmark calculation is presented for the quantum dynamics of tunnelling through a multidimensional asymmetric double well potential. A model Hamiltonian is used with a 1-dimensional tunnelling mode coupled to an $(M-1)$-dimensional harmonic bath, a system-bath problem. The benchmark calculation uses a basis set expansion of the wavefunction, with separate basis functions for the system and bath. Indistinguishability of configurations is exploited to greatly reduce the expense of the calculation, and a fully converged result is achieved. Comparison is offered to existing quantum dynamical methods that have tested this model problem, and further benchmark results not previously studied are presented.

1. Introduction

Tunnelling is a fundamentally quantum feature, absent from classical dynamics calculations and only partially treated by semi-classical ones [1]. Tunnelling events are vital for many processes in biology, chemistry and physics, including hydrogen tunnelling in enzyme catalysis [2,3], proton transfer in proteins [4], tunnelling through a reaction barrier [5], and atomic tunnelling of a Bose-Einstein condensate in a double well trap [6,7]. In order to correctly treat the dynamics of tunnelling problems, fully quantum techniques must be used.

Over the previous few decades there has been a growth in the number of time-dependent quantum dynamics methods appearing in the literature. Early examples include powerful integrators capable of solving the time-dependent Schrödinger equation exactly, such as the split-operator [8,9], Chebyshev expansion [10] and short iterative Lanczos [11] methods. However, these are only capable of treating a few degrees of freedom due to the exponential basis scaling effect. More recently we have schemes that are capable of treating a greater number of degrees of freedom. The multi-configurational time-dependent Hartree (MCTDH) method [12] in particular has emerged as a very accurate method of wavepacket propagation. It still suffers from exponential scaling, but with a smaller base to be exponentiated than the integrators mentioned above. Methods capable of scaling more favourably with dimensionality utilise GAUSSIAN wavepacket basis sets; examples of which include the full multiple spawning (FMS) [13] and matching pursuit split-operator Fourier transform (MP/SOFT) [14] methods, along with our own coupled coherent states (CCS) method [15]. Due to reliance on random basis sets, these methods suffer from noise and slow convergence, but they are all capable of treating problems in a fully quantum manner and have been applied to multidimensional tunnelling problems [16–19].

For any quantum dynamical method, existing or emerging, reliable benchmarks are required to assess their accuracy. A model Hamiltonian exhibiting tunnelling dynamics through a multidimensional asymmetric double well potential has been used as a test by the MP/SOFT [18] and CCS methods [19] mentioned above, and also more recently by a configuration interaction (CI) expansion method [20] and two-layer version of CCS (2L-CCS). [21] The Hamiltonian consists of a 1-dimensional tunnelling mode coupled to an $(M-1)$-dimensional harmonic bath, hence it is a system-bath problem which bears some similarity to the Caldeira-Leggett model of tunnelling in a dissipative system [22,23]. This Hamiltonian is non-dissipative, however and the harmonic modes all have the same frequency. System-bath models play an important role in physics, being used to describe superconductivity at a Josephson junction in a superconducting quantum interface device (SQUID) [24], for which the Caldeira-Leggett model provides a theoretical basis, and magnetic and conductance phenomena in the spin-bath regime [25].

No standard reference result has thus far been proposed for the model problem, and instead comparison to other methods and

* Corresponding author.
E-mail addresses: cmjg@leeds.ac.uk (J.A. Green), d.shalashilin@leeds.ac.uk (D.V. Shalashilin).

http://dx.doi.org/10.1016/j.cplett.2015.10.073
0009-2614/

indication of any sort of tunnelling has been used to evaluate their effectiveness. In this letter a benchmark result will be presented for the model Hamiltonian to evaluate its treatment by existing methods and provide a point of comparison for any future methods that wish to use it. Previously a 20-dimensional case has been considered that will also be presented here, alongside more challenging cases of 40 and 80-dimensions and 20-dimensions with a stronger system-bath coupling. We state from the outset that although the calculations performed in this work are relatively straightforward and trivial, they have not been published before and serve as a useful standalone reference to a problem tackled a number of times. Atomic units are used throughout, with $\hbar$=1.

2. Numerical details

2.1. Hamiltonian

The model Hamiltonian consists of a 1-dimensional tunnelling mode coupled to an $(M-1)$-dimensional bath. It is given by

$$\hat{H} = \frac{\hat{p}^{(1)^2}}{2} - \frac{\hat{q}^{(1)^2}}{2} + \frac{\hat{q}^{(1)^4}}{16\eta} + \frac{\hat{\mathbf{P}}^2}{2} + \frac{\left(1+\lambda\hat{q}^{(1)}\right)\hat{\mathbf{Q}}^2}{2} \tag{1}$$

where $(\hat{q}^{(1)}, \hat{p}^{(1)})$ are the position and momentum operators of the 1-dimensional tunnelling mode and $(\hat{\mathbf{Q}}, \hat{\mathbf{P}})$ are the position and momentum operators of the $(M-1)$-dimensional bath modes, with $\hat{\mathbf{Q}} = \sum_{l=2}^{M} \hat{q}^{(l)}$ and $\hat{\mathbf{P}} = \sum_{l=2}^{M} \hat{p}^{(l)}$. Previous studies have considered the case of a 20-dimensional problem, M = 20, system-bath coupling constant λ = 0.1 and potential parameter η = 1.3544. We shall also use these parameters initially before moving onto more challenging cases of M = 20, λ = 0.2 and M = 40 and M = 80 with λ = 0.1.

2.2. Quantum dynamics

The wavefunction is represented as a basis set expansion

$$|\Psi(t)\rangle = \sum_{j=1}^{N_{\text{bth}}} \sum_{n=1}^{N_{\text{sys}}} c_{jn}(t) |\psi_j^{\text{b}}\rangle\, |\psi_n^{\text{s}}\rangle, \tag{2}$$

in which $c_{jn}(t)$ are complex, time-dependent amplitudes, $|\psi_j^{\text{b}}\rangle$ is a time-independent basis function for the bath modes and $|\psi_n^{\text{s}}\rangle$ is a time-independent basis function for the system mode. The number of bath and system basis functions are given by N_{bth} and N_{sys} respectively. Substitution into the time-dependent Schrödinger equation leads to an equation for the time-dependence of the amplitudes

$$\frac{\mathrm{d}c_{im}(t)}{\mathrm{d}t} = -i \sum_{j=1}^{N_{\text{bth}}} \sum_{n=1}^{N_{\text{sys}}} H_{imjn} c_{jn}(t), \tag{3}$$

where H_{imjn} is the Hamiltonian matrix

$$\begin{aligned} H_{imjn} &= \langle \psi_i^{\text{b}} \psi_m^{\text{s}} | \hat{H} | \psi_j^{\text{b}} \psi_n^{\text{s}} \rangle \\ &= \langle \psi_m^{\text{s}} \left| \frac{\hat{p}^{(1)^2}}{2} - \frac{\hat{q}^{(1)^2}}{2} + \frac{\hat{q}^{(1)^4}}{16\eta} \right| \psi_n^{\text{s}} \rangle\, \delta_{ij} \\ &\quad + \langle \psi_i^{\text{b}} \left| \frac{\hat{\mathbf{P}}^2}{2} + \frac{\hat{\mathbf{Q}}^2}{2} \right| \psi_j^{\text{b}} \rangle\, \delta_{mn} + \frac{\lambda}{2} \langle \psi_i^{\text{b}} \left| \hat{\mathbf{Q}}^2 \right| \psi_j^{\text{b}} \rangle \langle \psi_m^{\text{s}} \left| \hat{q}^{(1)} \right| \psi_n^{\text{s}} \rangle. \end{aligned} \tag{4}$$

The bath and system basis functions are orthonormal (see below), a fact that has been exploited in the above.

The basis functions for the system are those of a particle in a rectangular box

$$\langle q^{(1)} | \psi_n^{\text{s}} \rangle = \sqrt{\frac{2}{L}} \sin\left(\frac{n\pi}{L} (q^{(1)} - q_{\text{box}}) \right), \tag{5}$$

where L is the size and q_{box} the lower coordinate of the box. Both these values may be adjusted to ensure a large enough area of coordinate space is sampled by the system basis functions.

The bath modes are nearly harmonic, therefore they can be represented by harmonic oscillator basis functions. A complete description of the bath would involve all excited state harmonic oscillator configurations, however in practice we can simply add on configurations until a converged result is achieved. For an $(M-1)$-dimensional bath, an excited state is comprised of the product of $(M-1)$ single particle harmonic oscillator functions, $\prod_{l=2}^{M} |\chi^{(l)}\rangle$, with different permutations of this product yielding different configurations. As the coupling of system and bath modes is proportional to $\hat{\mathbf{Q}}^2$ and all bath modes are initially in the ground state, only even excitations are involved.

The size of the bath basis can be reduced further by exploiting the effective indistinguishability of the bath modes. The amplitudes of the harmonic oscillator excited state configurations, which correspond to similar vibrational excitations but differ only by the bath modes involved, will be identical for a given excited state. This means that configurations corresponding to the same excited state can be grouped together and associated with a single amplitude. This simplification reflects the permutational symmetry of the Hamiltonian in Eq. (1), with the harmonic bath modes all having the same frequency. For example, if we include all even excitations up to a total quanta of 8 (the reasons for this choice will become apparent later), then the bath basis functions obtained by grouping configurations are:

$$\begin{aligned}
|\psi_1^{\text{b}}\rangle &= |0000\ldots0000\rangle \\
|\psi_2^{\text{b}}\rangle &= (|2000\ldots0000\rangle + \ldots + |0000\ldots0002\rangle)1/\sqrt{M-1} \\
|\psi_3^{\text{b}}\rangle &= (|4000\ldots0000\rangle + \ldots + |0000\ldots0004\rangle)1/\sqrt{M-1} \\
|\psi_4^{\text{b}}\rangle &= (|2200\ldots0000\rangle + \ldots + |0000\ldots0022\rangle) \times \sqrt{2!}/\sqrt{(M-1)(M-2)} \\
|\psi_5^{\text{b}}\rangle &= (|6000\ldots0000\rangle + \ldots + |0000\ldots0006\rangle)/\sqrt{M-1} \\
|\psi_6^{\text{b}}\rangle &= (|4200\ldots0000\rangle + \ldots + |0000\ldots0024\rangle) \times 1/\sqrt{(M-1)(M-2)} \\
|\psi_7^{\text{b}}\rangle &= (|2220\ldots0000\rangle + \ldots + |0000\ldots0222\rangle) \\
&\quad \times \sqrt{3!}/\sqrt{(M-1)(M-2)(M-3)} \\
|\psi_8^{\text{b}}\rangle &= (|8000\ldots0000\rangle + \ldots + |0000\ldots0008\rangle)/\sqrt{M-1} \\
|\psi_9^{\text{b}}\rangle &= (|6200\ldots0000\rangle + \ldots + |0000\ldots0026\rangle) \times 1/\sqrt{(M-1)(M-2)} \\
|\psi_{10}^{\text{b}}\rangle &= (|4400\ldots0000\rangle + \ldots + |0000\ldots0044\rangle) \times \sqrt{2!}/\sqrt{(M-1)(M-2)} \\
|\psi_{11}^{\text{b}}\rangle &= (|4220\ldots0000\rangle + \ldots + |0000\ldots0224\rangle) \times \sqrt{2!}/\sqrt{(M-1)(M-2)(M-3)} \\
|\psi_{12}^{\text{b}}\rangle &= (|2222\ldots0000\rangle + \ldots + |0000\ldots2222\rangle) \\
&\quad \times \sqrt{4!}/\sqrt{(M-1)(M-2)(M-3)(M-4)}
\end{aligned} \tag{6}$$

with relevant normalisation factors included. The square of the normalisation factors is simply equal to the number of configurations grouped; in this case there are 8855 bath configurations governed by only 12 distinct bath basis functions, and hence 12 distinct amplitudes. Such reduction of parameters due to indistinguishability of modes/particles and permutational symmetry of the Hamiltonian is well known and exploited by the second quantization approach. Here the idea is used in a more straightforward fashion.

2.3. Matrix elements

Now the basis functions have been defined, the matrix elements of the Hamiltonian may be evaluated. Firstly, the system elements

$$\begin{aligned}\langle\psi_m^{\mathrm{s}}\left|\frac{\hat{p}^{(1)^2}}{2}-\frac{\hat{q}^{(1)^2}}{2}+\frac{\hat{q}^{(1)^4}}{16\eta}\right|\psi_n^{\mathrm{s}}\rangle \\ =\frac{n^2\pi^2}{2L^2}\delta_{mn} \quad +\frac{2}{L}\int_{q_{\mathrm{box}}}^{q_{\mathrm{box}}+L}\sin\left(\frac{m\pi}{L}(q^{(1)}-q_{\mathrm{box}})\right) \\ \times\sin\left(\frac{n\pi}{L}(q^{(1)}-q_{\mathrm{box}})\right)\left(\frac{q^{(1)^4}}{16\eta}-\frac{q^{(1)^2}}{2}\right)\mathrm{d}q^{(1)},\end{aligned} \tag{7}$$

are the particle in a box energy levels, plus an additional potential term. Secondly, the bath elements

$$\langle\psi_i^{\mathrm{b}}|\frac{\hat{\mathbf{P}}^2}{2}+\frac{\hat{\mathbf{Q}}^2}{2}|\psi_j^{\mathrm{b}}\rangle=\delta_{ij}\left(\sum_{l=2}^{M}\epsilon_i^{(l)}+\frac{M-1}{2}\right) \tag{8}$$

are simply the harmonic oscillator eigenvalues for the excited states, where $\epsilon_i^{(l)}$ is the number of quanta in one mode. Finally, the system-bath interaction elements are comprised of a system term multiplied by a bath term, and are given by

$$\begin{aligned}\langle\psi_m^{\mathrm{s}}|\hat{q^{(1)}}|\psi_n^{\mathrm{s}}\rangle=\frac{2}{L}\int_{q_{\mathrm{box}}}^{q_{\mathrm{box}}+L}\sin\left(\frac{m\pi}{L}(q^{(1)}-q_{\mathrm{box}})\right) \\ \times\sin\left(\frac{n\pi}{L}(q^{(1)}-q_{\mathrm{box}})\right)q^{(1)}\,\mathrm{d}q^{(1)}.\end{aligned} \tag{9}$$

2.4. Initial values

As with previous studies, the initial wavepacket is defined by

$$\langle q|\Psi(0)\rangle=\left(\frac{1}{\pi}\right)^{\frac{M}{4}}\prod_{l=1}^{M}\exp\left(-\frac{1}{2}\left(q^{(l)}-q^{(l)}(0)\right)^2\right), \tag{12}$$

where the initial tunnelling coordinate $q^{(1)}(0)=-2.5$ is located in the lower well, and initial bath coordinates $q^{(l)}(0)=0.0$ for $l>1$. The initial momenta for all modes is $p^{(l)}(0)=0.0$. Thus, the initial conditions for all bath modes are identical, which along with their identical Hamiltonian parameters makes them indistinguishable.

The initial amplitudes are calculated via projection onto the initial wavepacket, with all bath modes in the ground level at $t=0$

$$\begin{aligned}c_{im}(0)= & \langle\psi_i^{\mathrm{b}}\psi_m^{s}|\Psi(0)\rangle=\delta_{1m}\langle\psi_m^{s}|\Psi(0)\rangle \\ = & \delta_{1m}\sqrt{\frac{2}{L}}\int_{q_{\mathrm{box}}}^{q_{\mathrm{box}}+L}\sin\left(\frac{m\pi}{L}(q^{(1)}-q_{\mathrm{box}})\right)\left(\frac{1}{\pi}\right)^{\frac{1}{4}} \\ & \times\exp\left(-\frac{1}{2}\left(q^{(1)}-q^{(1)}(0)\right)^2\right)\mathrm{d}q^{(1)}.\end{aligned} \tag{13}$$

3. Results

The quantity of interest is the cross-correlation function (CCF) between the wavefunction at time t and the mirror image of the initial wavepacket, $|\bar{\Psi}(0)\rangle$. The mirror image of the initial state is located in the upper well of the asymmetric potential, therefore non-zero values of the CCF are indicative of tunnelling. Rather than express $|\bar{\Psi}(0)\rangle$ as a GAUSSIAN wavepacket in the CCF, it is simpler to represent it as the basis set expansion instead, with initial amplitudes calculated using the mirror image coordinates (i.e. $\bar{q}^{(1)}(0)=+2.5$)

$$\langle\psi_i^{\mathrm{b}}|\hat{\mathbf{Q}}^2|\psi_j^{\mathrm{b}}\rangle=\begin{cases}\frac{A_{ij}}{2}\sqrt{(\epsilon_i^{(l)}+2)(\epsilon_i^{(l)}+1)} & \text{if } \epsilon_i^{(l)}=\epsilon_j^{(l)}-2 \text{ in only one mode and } \epsilon_i^{(l)}=\epsilon_j^{(l)} \text{ in all other modes}\\ \frac{A_{ij}}{2}\sqrt{\epsilon_i^{(l)}(\epsilon_i^{(l)}-1)} & \text{if } \epsilon_i^{(l)}=\epsilon_j^{(l)}+2 \text{ in only one mode and } \epsilon_i^{(l)}=\epsilon_j^{(l)} \text{ in all other modes}\\ \sum_{l=2}^{M}\epsilon_i^{(l)}+\frac{M-1}{2} & \text{if } \epsilon_i^{(l)}=\epsilon_j^{(l)} \text{ in all modes}\\ 0 & \text{if states differ by more than two quanta in one mode, or two quanta in more than one mode}\end{cases} \tag{10}$$

For the bath term, A_{ij} is a constant that depends upon the normalisation factors and the number of configurations that differ by only two quanta in one mode between excited states. Returning to the example of including all even excitations up to and including a total quanta of 8, we may evaluate the $\langle\psi_i^{\mathrm{b}}|\hat{\mathbf{Q}}^2|\psi_j^{\mathrm{b}}\rangle$ matrix elements to clarify what these A_{ij} constants are:

$$\begin{array}{c}\\ \langle\psi_1^{\mathrm{b}}|\\ \langle\psi_2^{\mathrm{b}}|\\ \langle\psi_3^{\mathrm{b}}|\\ \langle\psi_4^{\mathrm{b}}|\\ \langle\psi_5^{\mathrm{b}}|\\ \langle\psi_6^{\mathrm{b}}|\\ \langle\psi_7^{\mathrm{b}}|\\ \langle\psi_8^{\mathrm{b}}|\\ \langle\psi_9^{\mathrm{b}}|\\ \langle\psi_{10}^{\mathrm{b}}|\\ \langle\psi_{11}^{\mathrm{b}}|\\ \langle\psi_{12}^{\mathrm{b}}|\end{array}\begin{array}{c}\begin{array}{cccccccccccc}|\psi_1^{\mathrm{b}}\rangle & |\psi_2^{\mathrm{b}}\rangle & |\psi_3^{\mathrm{b}}\rangle & |\psi_4^{\mathrm{b}}\rangle & |\psi_5^{\mathrm{b}}\rangle & |\psi_6^{\mathrm{b}}\rangle & |\psi_7^{\mathrm{b}}\rangle & |\psi_8^{\mathrm{b}}\rangle & |\psi_9^{\mathrm{b}}\rangle & |\psi_{10}^{\mathrm{b}}\rangle & |\psi_{11}^{\mathrm{b}}\rangle & |\psi_{12}^{\mathrm{b}}\rangle\end{array}\\ \begin{pmatrix}\frac{M-1}{2} & \frac{\sqrt{2(M-1)}}{2} & 0 & 0 & 0 & 0 & 0 & 0 & 0 & 0 & 0 & 0\\ \frac{\sqrt{2(M-1)}}{2} & 2+\frac{M-1}{2} & \sqrt{3} & \sqrt{M-2} & 0 & 0 & 0 & 0 & 0 & 0 & 0 & 0\\ 0 & \sqrt{3} & 4+\frac{M-1}{2} & 0 & \frac{1}{2}\sqrt{30} & \frac{\sqrt{2(M-2)}}{2} & 0 & 0 & 0 & 0 & 0 & 0\\ 0 & \sqrt{M-2} & 0 & 4+\frac{M-1}{2} & 0 & \sqrt{6} & \frac{\sqrt{6(M-3)}}{2} & 0 & 0 & 0 & 0 & 0\\ 0 & 0 & \frac{1}{2}\sqrt{30} & 0 & 6+\frac{M-1}{2} & 0 & 0 & \frac{1}{2}\sqrt{56} & \frac{\sqrt{2(M-2)}}{2} & 0 & 0 & 0\\ 0 & 0 & \frac{\sqrt{2(M-2)}}{2} & \sqrt{6} & 0 & 6+\frac{M-1}{2} & 0 & 0 & \frac{1}{2}\sqrt{30} & \frac{1}{2}\sqrt{24} & \sqrt{M-3} & 0\\ 0 & 0 & 0 & \frac{\sqrt{6(M-3)}}{2} & 0 & 0 & 6+\frac{M-1}{2} & 0 & 0 & 0 & \frac{1}{2}\sqrt{36} & \sqrt{2(M-4)}\\ 0 & 0 & 0 & 0 & \frac{1}{2}\sqrt{56} & 0 & 0 & 8+\frac{M-1}{2} & 0 & 0 & 0 & 0\\ 0 & 0 & 0 & 0 & \frac{\sqrt{2(M-2)}}{2} & \frac{1}{2}\sqrt{30} & 0 & 0 & 8+\frac{M-1}{2} & 0 & 0 & 0\\ 0 & 0 & 0 & 0 & 0 & \frac{1}{2}\sqrt{24} & 0 & 0 & 0 & 8+\frac{M-1}{2} & 0 & 0\\ 0 & 0 & 0 & 0 & 0 & \sqrt{M-3} & \frac{1}{2}\sqrt{36} & 0 & 0 & 0 & 8+\frac{M-1}{2} & 0\\ 0 & 0 & 0 & 0 & 0 & 0 & \sqrt{2(M-4)} & 0 & 0 & 0 & 0 & 8+\frac{M-1}{2}\end{pmatrix}\end{array} \tag{11}$$

$$\mathrm{CCF}(t) = \langle\bar{\Psi}(0)|\Psi(t)\rangle = \sum_{i,j=1}^{N_{\mathrm{bth}}}\sum_{m,n=1}^{N_{\mathrm{sys}}} \bar{c}^{*}_{im}(0)c_{jn}(t)\langle\psi^{\mathrm{b}}_{i}\psi^{\mathrm{s}}_{m}|\psi^{\mathrm{b}}_{j}\psi^{\mathrm{s}}_{n}\rangle$$
$$= \sum_{i,j=1}^{N_{\mathrm{bth}}}\sum_{m,n=1}^{N_{\mathrm{sys}}} \bar{c}^{*}_{im}(0)c_{jn}(t)\delta_{ij}\delta_{mn}$$
$$= \sum_{j=1}^{N_{\mathrm{bth}}}\sum_{n=1}^{N_{\mathrm{sys}}} \bar{c}^{*}_{jn}(0)c_{jn}(t). \qquad (14)$$

To aid with comparisons made later in the text, the spectra of the CCFs are presented via a Fourier transform (FT):

$$I(\omega) = \int_{0}^{T} \mathrm{Re}(\mathrm{CCF}(t))\exp(-i\omega t)\,\mathrm{d}t. \qquad (15)$$

The FT also makes it simpler to identify the long-time propagation accuracy of a quantum dynamical method, due to a small number of sharp peaks as opposed to the highly oscillatory nature of the CCF. Total propagation time is $T = 120$ a.u for all results that follow, with step size $\delta t = 0.001$ a.u.

3.1. 20D

3.1.1. $\lambda = 0.1$

The calculation can be converged with respect to the system box length L (to ensure sufficient coordinate space sampling of the tunnelling mode and allow correct representation of the initial wavepacket), number of system basis functions N_{sys}, and number of bath basis functions N_{bth} (to ensure sufficient basis functions, and hence amplitudes, are included to represent the system and bath modes and their time-dependence over the timeframe of the calculation). The calculation is fully converged when the CCF and FT show no observable change upon increasing L, N_{sys} and N_{bth} in turn, whilst the other two parameters are held fixed at their fully converged value. Figures illustrating this are not included in the main body text of the letter as they are trivial, however they are included in Supplementary Material (Figs. S1–S3). The result of the fully converged benchmark calculation is shown in Figure 1, with the CCF in panel (a) and the FT in panel (b).

In the fully converged calculation the system box length is $L = 12$ and the lower coordinate of the box is $q_{\mathrm{box}} = 6$, meaning the system wavefunction at $t = 0$ a.u. until $t = 120$ a.u. samples coordinate space in the region $[-6:6]$. The number of system basis functions $N_{\mathrm{sys}} = 50$, and although this is a relatively small number only a single mode is being treated by them and they cover a large amount of coordinate space. This indicates a significant amount of delocalisation, as may be expected from a tunnelling mode, hence accurate treatment of the system by other methods may not be as trivial as for this benchmark calculation. The range of momentum values required to be sampled can be estimated from the wavelengths of the particle in a box basis functions and the De Broglie relationship. The longest wavelength basis function occurs when $n = 1$ in Eq. (5) and smallest when $n = N_{\mathrm{sys}}$. This gives a range of wavelengths from $\lambda = 2L$ and $\lambda = 2L/N_{\mathrm{sys}}$, leading to momenta of $p = \pi/L$ and $p = \pi N_{\mathrm{sys}}/L$. Therefore as well as a significant amount of coordinate space, a large amount of momentum space must also be sampled.

The number of bath basis functions $N_{\mathrm{bth}} = 12$, corresponding to adding on even excited harmonic oscillator states up to and including 8 quanta. The explicit form of these basis functions has been demonstrated in Eq. (6). Whilst this may not seem like a very large amount, we can recall the simplification we made earlier: all configurations for a particular excited state are governed by the same amplitude. So we have 8855 configurations governed by only 12 bath basis functions – a significant reduction. Taking into account that the number of system basis functions $N_{\mathrm{sys}} = 50$, the total wavefunction is a superposition of 50×8855 configurations, described by only 50×12 amplitudes. For calculations where this trick is not possible, a large amount of basis functions may be required for accurate modelling of the wavefunction, requiring a large amount of phase space to be sampled.

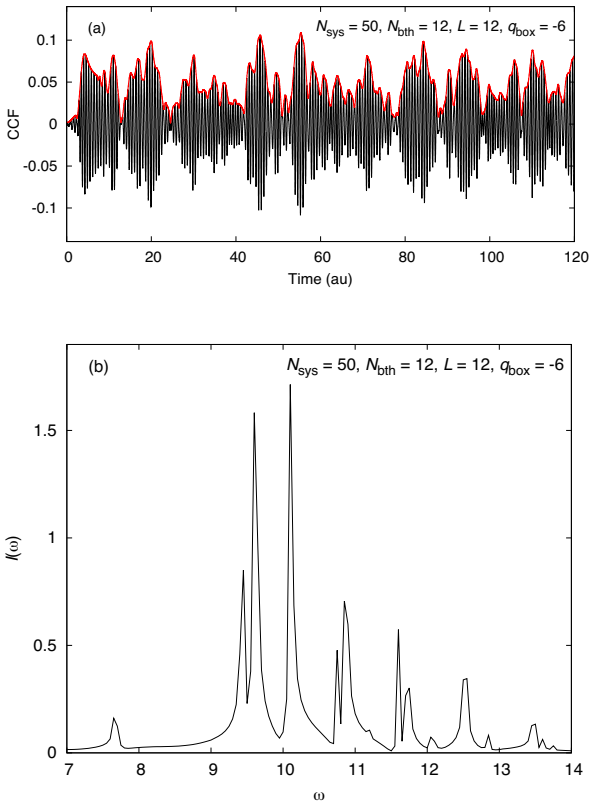

Figure 1. Fully converged benchmark calculation for the 20D, $\lambda = 0.1$ case, with the real parts (black lines) and moduli (red lines) of the cross-correlation function in panel (a) and the Fourier transform of the real parts in panel (b). (For interpretation of the references to color in this figure legend, the reader is referred to the web version of the article.)

Comparison of our benchmark calculation to previous works on this Hamiltonian [18–21] is shown in Figures 2 and 3. Evaluating each of the methods in turn, MP/SOFT in panel (a) has done a reasonable job for short time propagation, although there is a loss of structure and amplitude in the CCF at longer times. This suggests that the calculation is less able to treat tunnelling as the propagation progresses, producing a more semiclassical result. In panel (b) the CCS calculation from Ref. [19] does not reproduce the converged result, missing the large peak splitting in the FT at $\omega = 9.5$, as well as the smaller splittings at $\omega = 10.8$ and $\omega = 11.6$. Additionally, there is a peak at $\omega = 9.0$ which does not appear in the benchmark calculation. Some indication as to why this is the case may be found in Ref. [19], where it was noted that the bath modes were sampled from a narrow distribution. Based on the results of this benchmark calculation, where a number of excited harmonic oscillator states were required for the bath, a broader distribution may be required. In Ref. [21] corrected CCS calculations with better and broader sampling of the bath has been reported, and this is shown in panel (c). The re-calculated CCS result performs much better, with the CCF and FT more closely resembling the benchmark calculation. The CI expansion performs best out of all three methods in panel (d), with a CCF that is accurate with respect to the benchmark for a longer time than MP/SOFT and CCS, leading to a FT that is also more accurate. This is to be expected as the CI expansion is similar to our

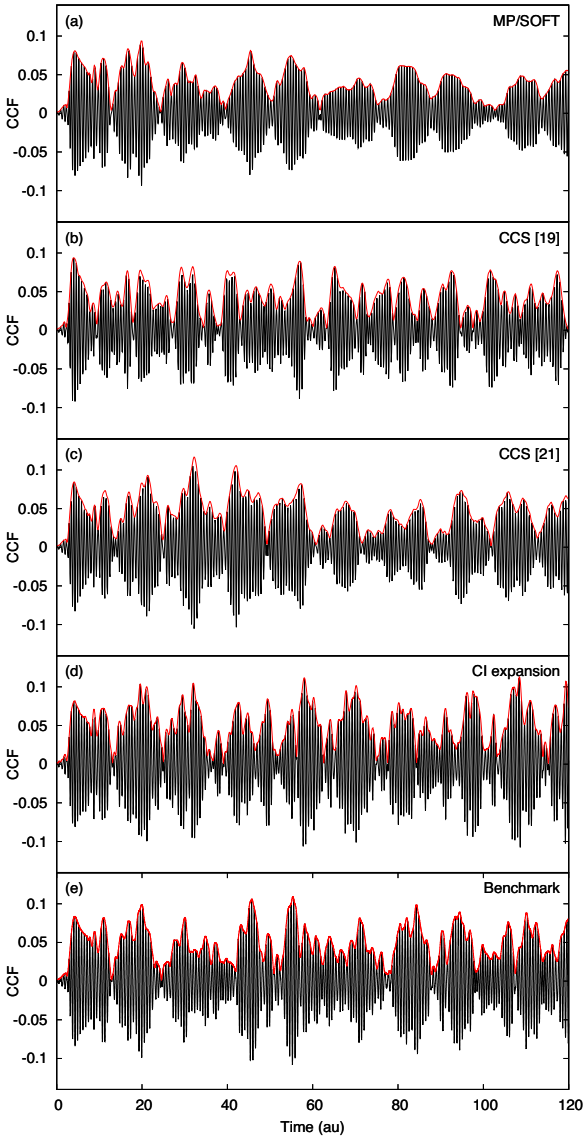

Figure 2. Comparison of the real parts (black lines) and moduli (red lines) of the cross-correlation functions for the MP/SOFT, CCS and CI expansion methods to the benchmark. Two CCS results are presented, that from Ref. [19] in panel (b) and the re-calculated version from Ref. [21] in panel (c). Parameters for benchmark are equal to the fully converged case: $L = 12$, $q_{box} = -6$, $N_{sys} = 50$ and $N_{bth} = 12$. (For interpretation of the references to color in this figure legend, the reader is referred to the web version of the article.)

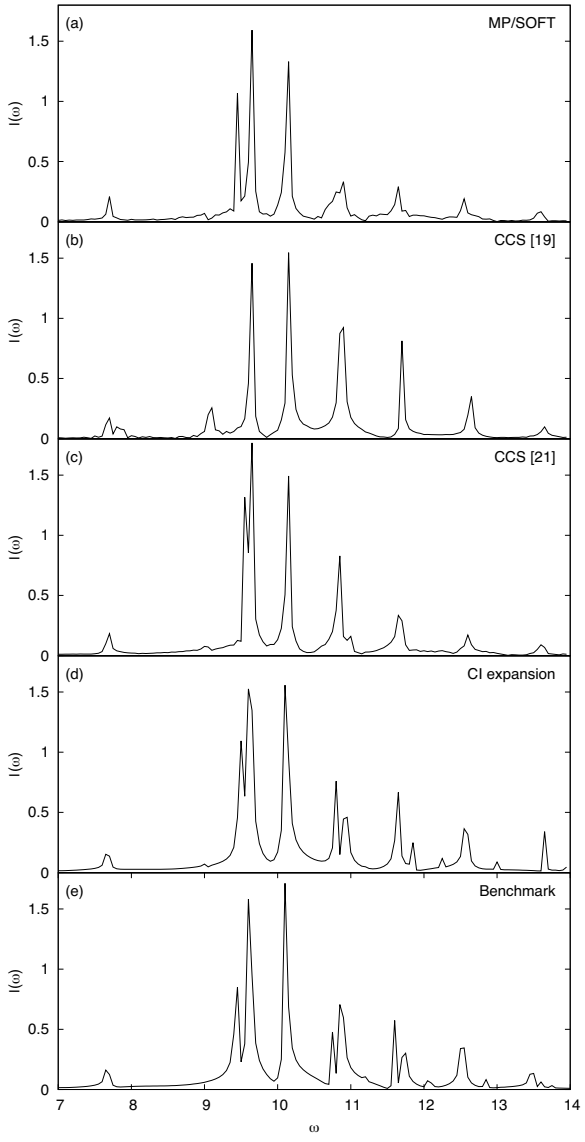

Figure 3. Comparison of Fourier transforms of the real cross-correlation functions for the MP/SOFT, CCS and CI expansion methods to the benchmark. Two CCS results are presented, that from Ref. [19] in panel (b) and the re-calculated version from Ref. [21] in panel (c). Parameters for benchmark are equal to the fully converged case: $L = 12$, $q_{box} = -6$, $N_{sys} = 50$, $N_{bth} = 12$.

benchmark calculation, with a basis set expansion based on excited levels used for modelling of the modes. Furthermore, the CI expansion method uses a regular basis unlike CCS and MP/SOFT, and is therefore free from the problem of random noise.

3.1.2. $\lambda = 0.2$

The $\lambda = 0.2$ case has not been explored by any previous work, but it would present a more stringent test for a quantum dynamical method as the increase in coupling between system and bath will cause greater perturbation of the bath by the system. One would therefore expect an increased number of bath basis functions required for convergence in the calculation. The fully converged result is shown in Figure 4, with the CCF in panel (a) and the FT in panel (b). Figures illustrating how this calculation converges are included in Supplementary Material (Figs. S4–S6), as with the 20D, $\lambda = 0.1$ case.

The system box size L is the same as for the $\lambda = 0.1$ case, and the number of system basis functions required is also the same. Therefore the tunnelling mode is as delocalised as for the $\lambda = 0.1$ case, requiring no further sampling of phase space over the timeframe of the calculation. The increase in complexity arises with the modelling of the bath, as a much greater number of bath basis functions are required with $N_{bth} = 45$. This corresponds to involving excited levels up to and including 14 quanta. Without exploiting the indistinguishability of the excited state configurations, an extremely large number of basis functions would be required; in this result there are 657 800 bath configurations governed by only 45 basis functions. The total wavefunction is a superposition of the $50 \times 657\,800$ configurations, which can be described by only 50×45 independent amplitudes. As expected, this strongly coupled system and bath illustrates the significant perturbation of the bath by the system due to the large number of bath configurations required for convergence. Calculations with even larger λ turned

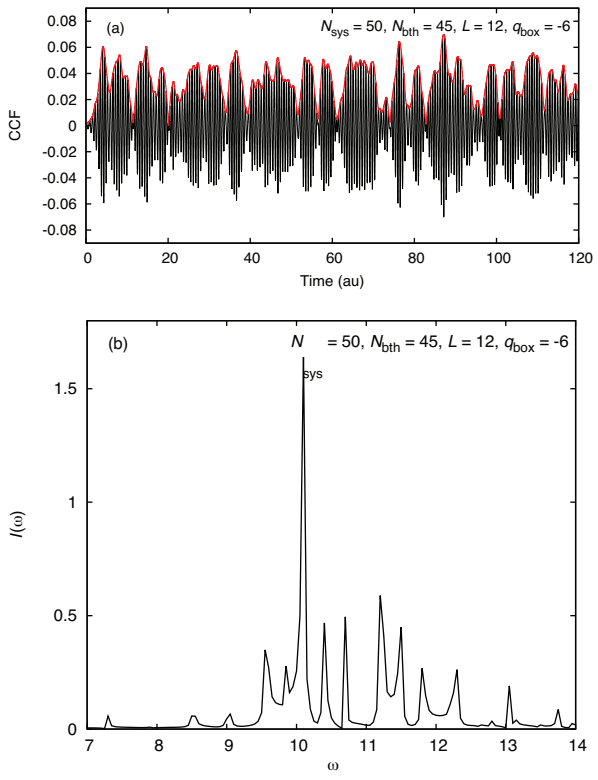

Figure 4. Fully converged benchmark calculation for the 20D, λ = 0.2 case, with the real parts (black lines) and moduli (red lines) of the cross-correlation function in panel (a) and the Fourier transform of the real parts in panel (b). (For interpretation of the references to color in this figure legend, the reader is referred to the web version of the article.)

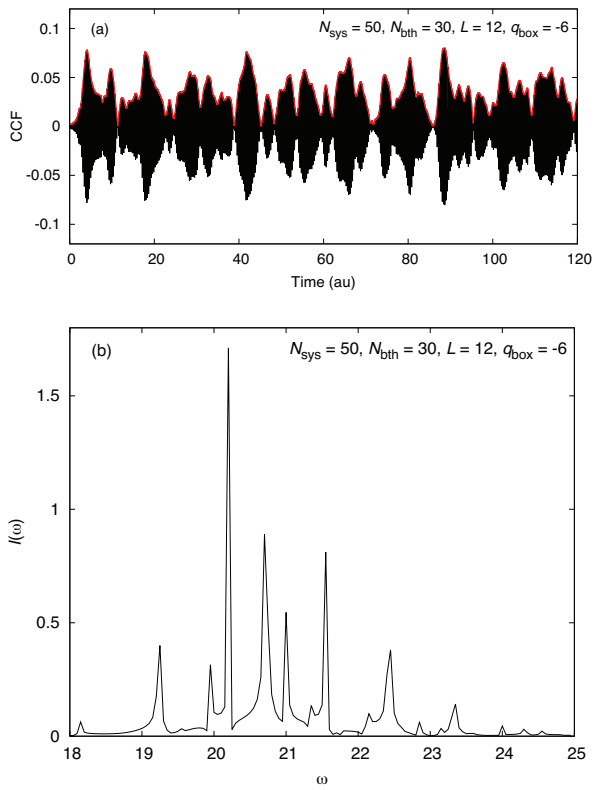

Figure 5. Fully converged benchmark calculation for the 40D, λ = 0.1 case, with the real parts (black lines) and moduli (red lines) of the cross-correlation function in panel (a) and the Fourier transform of the real parts in panel (b). (For interpretation of the references to color in this figure legend, the reader is referred to the web version of the article.)

out to be impossible because increasing coupling between system and bath modes makes the asymmetric potential unbound.

3.2. 40D & 80D

We have also performed calculations for 40D and 80D cases, i.e. with 39 and 79 bath modes in the Hamiltonian in Eq. (1). There is no obvious computational scaling with dimensionality for the benchmark calculation as the bath basis functions represent excited states of the entire system rather than individual modes. However, a greater number of excited states may be required due to the increase in dimensionality of the bath. We revert to the weak coupling case of λ = 0.1 for this reason, as an increase in the number of bath modes and their coupling may result in a calculation that is prohibitively expensive to converge, even when exploiting mode indistinguishabilities.

The fully converged result for the 40D case is shown in Figure 5, with the CCF in panel (a) and the FT in panel (b). Once more, figures illustrating how this calculation converges are included in Supplementary Material (Figs. S7–S9). It can be seen that the CCF oscillates at a higher frequency than the 20D, λ = 0.1 case, which is demonstrated in the FT with a shift to higher frequencies. This is due to the tunnelling coordinate $q^{(1)}$ being coupled to all of the bath modes, and there is a greater number of bath modes for the 40D case than the 20D case. As the dimensionality increases, so does the separation between the two wells [18], therefore one would expect a decrease in the amount of quantum tunnelling. By comparison of the CCF's for the 20D and 40D case in Figures 1a and 5a, we see a small decrease in the amplitude for the 40D case, indicative of a small decrease in the amount of tunnelling.

For the 80D case, the fully converged result is shown in Figure 6, with the CCF in panel (a) and the FT in panel (b). Illustration of convergence is shown in Supplementary Material (Figs. S10–S12). There is a large decrease in the amplitude of the CCF compared to the 20D and 40D cases, indicating a large decrease in the amount of quantum tunnelling due to the increase in separation of the wells. As with the 40D case, the frequency of tunnelling increases because of coupling to a larger number of bath modes which can be observed from the CCF, or more directly from the FT.

For both the 40D and 80D cases, the number of system basis functions required for convergence does not increase from the 20D case. Therefore, even though the tunnelling mode is coupled to more bath modes, more system basis functions are not required. The size of the box required for the system basis functions does not increase for the 40D case relative to 20D; however there is a small increase for the 80D case, meaning a small increase in the amount of coordinate space required to be sampled by the tunnelling mode. As the increased dimensionality will result in bath modes that cover a larger amount of coordinate space, and the fact that the tunnelling mode is coupled to all of them, this can be explained. The most significant change for both the 40D and 80D cases when compared to the 20D case is the number of bath basis functions required. For the 40D case N_{bth} = 30, corresponding to the bath basis functions involving excited levels up to and including 12 quanta. For the 80D case N_{bth} = 45, corresponding to the bath basis functions involving excited levels up to and including 14 quanta, the same as required for λ = 0.2. As expected, the increased dimensionality of the bath has required more excited levels to converge. The total wavefunction is a superposition of the 50 × 177 100 and 50 × 657 800 configurations for the 40D and 80D cases respectively, which is described by sets of only 50 × 30 and 50 × 45 independent amplitudes.

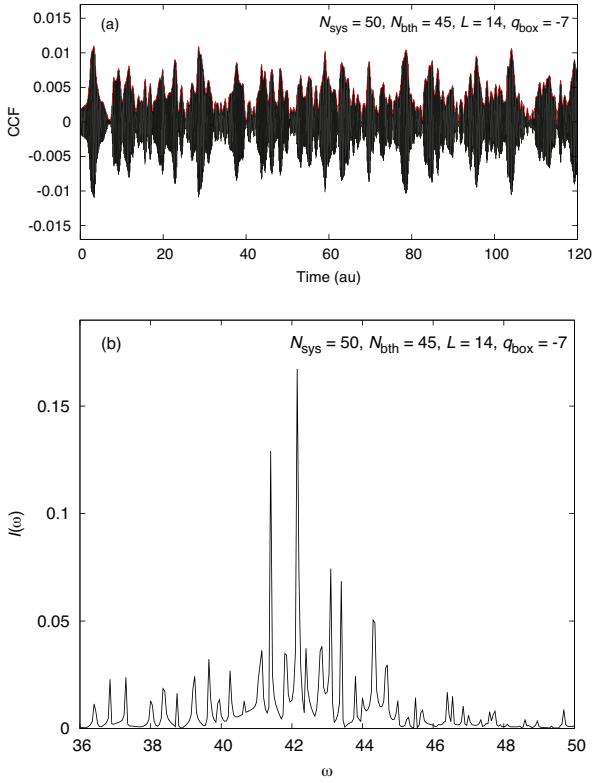

Figure 6. Fully converged benchmark calculation for the 80D, $\lambda = 0.1$ case, with the real parts (black lines) and moduli (red lines) of the cross-correlation function in panel (a) and the Fourier transform of the real parts in panel (b). (For interpretation of the references to color in this figure legend, the reader is referred to the web version of the article.)

4. Conclusions

A benchmark calculation has been presented for tunnelling through a multidimensional asymmetric double well potential. The model Hamiltonian, previously used by the MP/SOFT [18] CCS, [19,21] and CI expansion [20] methods, consists of a 1-dimensional system tunnelling mode coupled to an $(M-1)$-dimensional nearly harmonic bath; a system-bath problem. The dynamics were computed via a basis set expansion of the wavefunction, comprising of separate time-independent basis functions for the system and bath and associated time-dependent amplitudes. The basis functions for the system were those of a particle in a rectangular box, and those for the bath were ground and excited state harmonic oscillator configurations. The number of bath basis functions required to converge the calculation was reduced by noting two useful properties of this problem. Firstly, the coupling of bath and system is proportional to the square of the bath coordinate; therefore, as initially all modes are in the ground state, only even excited state harmonic oscillator functions were required. Secondly, and more significantly, the indistinguishability of the excited state configurations was exploited so that only one amplitude was required to be associated to each excited state and not one amplitude per configuration for each excited state.

A fully converged result for the 20D, $\lambda = 0.1$ problem has been presented, with comparison to the methods that have previously studied this Hamiltonian. The MP/SOFT and CI expansion methods compared well to the benchmark, whereas the CCS calculation from Ref. [19] did not due to insufficient sampling of the bath. However, a re-calculated CCS result in Ref. [21] with improved sampling performed much better. Guidance for sampling this problem has also been presented, with the tunnelling mode being highly delocalised and requiring a considerable amount of phase space to be sampled, as may be expected. Ranges for sampling the coordinates and momenta of the system have been given in Section 3.1.1. The bath required a large number of configurations for convergence, although it heavily benefited from the exploitation of indistinguishability to reduce the number of basis functions required in this calculation.

A stronger coupling case, not previously studied, of $\lambda = 0.2$ was computed and it was observed that the system did not need additional basis functions to accurately represent it, although the bath did due to increased perturbation by the system. Higher dimensional cases of 40D and 80D have also been presented, in the $\lambda = 0.1$ regime once more. As with the stronger coupling case, no increased treatment of the system was required, but additional basis functions were required for the bath. However, this is most likely due to the increased size of the bath rather than increased perturbation by the system. The fully converged CCFs and FTs for each of these calculations has been presented, providing a point of comparison for future tests on tunnelling/system-bath problems using this model Hamiltonian. The latter 40D and 80D cases, as well as 20D $\lambda = 0.2$, may present a challenge for the most advanced methods of multidimensional quantum dynamics. All data produced by the benchmark calculation in this letter has been included in Supplementary Material so that it may be used in future work.

The success of exploiting the indistinguishability of the bath basis function excited state configurations has provided motivation towards further studies in which indistinguishabilities are used to reduce the dimensionality of a problem. Using this model Hamiltonian as an example once more, if it were second quantized then the modes themselves would be indistinguishable rather than the excited state configurations of the bath basis functions. Investigations of this using the CCS method are currently underway.

Acknowledgements

This work was supported by the EPSRC grants No. EP/J019240/1 and EP/I014500/1. J. A. G. is supported by the University Research Scholarship from the University of Leeds. D.V.S. gratefully acknowledges V. Batista and S. Habershon for providing their data.

Appendix A. Supplementary data

Supplementary data associated with this article can be found, in the online version, at http://dx.doi.org/10.1016/j.cplett.2015.10.073.

References

[1] K.G. Kay, J. Chem. Phys. 107 (1997) 2313.
[2] Y. Cha, C. Murray, J. Klinman, Science 243 (1989) 1325.
[3] B.J. Bahnson, J.P. Klinman, in: D.L. Purich (Ed.), Enzyme Kinetics and Mechanism Part D: Developments in Enzyme Dynamics, volume 249 of Methods in Enzymology, Academic Press, 1995, p. 373.
[4] A. Kohen, R. Cannio, S. Bartolucci, J.P. Klinman, Nature 399 (1999) 496.
[5] M. Topaler, N. Makri, J. Chem. Phys. 101 (1994) 7500.
[6] G.J. Milburn, J. Corney, E.M. Wright, D.F. Walls, Phys. Rev. A 55 (1997) 4318.
[7] A. Smerzi, S. Fantoni, S. Giovanazzi, S.R. Shenoy, Phys. Rev. Lett. 79 (1997) 4950.
[8] M. Feit, A. Steiger, J. Comp. Phys. 47 (1982) 412.
[9] M.D. Feit, J.A. Fleck, J. Chem. Phys. 78 (1983) 301.
[10] H. Tal-Ezer, R. Kosloff, J. Chem. Phys. 81 (1984) 3967.
[11] T.J. Park, J.C. Light, J. Chem. Phys. 85 (1986) 5870.
[12] H.-D. Meyer, U. Manthe, L. Cederbaum, Chem. Phys. Lett. 165 (1990) 73.
[13] T.J. Martinez, M. Ben-Nun, R.D. Levine, J. Phys. Chem. 100 (1996) 7884.
[14] Y. Wu, V.S. Batista, J. Chem. Phys. 118 (2003) 6720.
[15] D.V. Shalashilin, M.S. Child, J. Chem. Phys. 113 (2000) 10028.
[16] M.D. Coutinho-Neto, A. Viel, U. Manthe, J. Chem. Phys. 121 (2004) 9207.
[17] M. Ben-Nun, T.J. Martnez, J. Chem. Phys. 112 (2000) 6113.

[18] Y. Wu, V.S. Batista, J. Chem. Phys. 121 (2004) 1676.
[19] P.A.J. Sherratt, D.V. Shalashilin, M.S. Child, Chem. Phys. 322 (2006) 127.
[20] S. Habershon, J. Chem. Phys. 136 (2012) 054109.
[21] J.A. Green, A. Grigolo, M. Ronto, D.V. Shalashilin, A two-layer approach to the coupled coherent states method, 2015 (Submitted for publication).
[22] A.O. Caldeira, A.J. Leggett, Phys. Rev. Lett. 46 (1981) 211.
[23] A. Caldeira, A. Leggett, Ann. Phys. 149 (1983) 374.
[24] Y. Makhlin, G. Schön, A. Shnirman, Rev. Mod. Phys. 73 (2001) 357.
[25] N.V. Prokof'ev, P.C.E. Stamp, Rev. Prog. Phys. 63 (2000) 669.